ELSEVIER

Journal of Alloys and Compounds 262–263 (1997) 381–389

Journal of ALLOYS AND COMPOUNDS

Structural properties of amorphous and nanocrystallized Fe-Cu-Nb-Si-B and Fe-Gd-Cu-Nb-Si-B ribbons

O. Crisan[a], J.M. Le Breton[b,*], A. Jianu[a], J. Teillet[b], G. Filoti[a]

[a] *Institute of Physics and Technology of Materials, P.O. Box MG-07, 76900 Bucharest-Magurele, Romania*
[b] *GMP Magnétisme et Applications, UMR 6634 CNRS-Université de Rouen, Faculté des Sciences, 76821 Mont-Saint-Aignan Cedex, France*

Abstract

The influence of Gd addition on the structural properties of Fe-Cu-Nb-Si-B nanocrystallized and amorphous alloys is studied. The crystallization temperature increases and the microstructure of the annealed samples changes. Gd addition induces the formation of Gd-Fe-B phases. In fully crystallized Fe-Gd-Cu-Nb-Si-B alloys the α-Fe(Si), Fe-Nb-B, $Gd_3Fe_{62}B_{14}$ and $Gd_{1.1}Fe_4B_4$ phases are observed. The evolution of the microstructure is followed as a function of the cumulative effects of annealing time and temperature. The results su gest the transformation of the metastable $Gd_3Fe_{62}B_{14}$ phase into $Gd_{1.1}Fe_4B_4$ and α-Fe. The hyperfine parameters of the $Gd_3Fe_{62}B_{14}$ Mössbauer contribution are reported. © 1997 Elsevier Science S.A.

Keywords: Fe-Cu-Nb-Si-B ribbons; Gd addition; M...t. spinning; Nanostructure; Mössbauer spectrometry

1. Introduction

In the last few years, a new type of nanocrystalline material, developed from Fe-Cu-Nb-Si-B amorphous ribbons, has been the subject of great interest [1–5] due to its remarkable soft magnetic properties. Appropriate annealing gives rise to a structure consisting of nanosized grains of α-Fe(Si) solid solution or DO_3-type Fe_3Si crystallites embedded into an amorphous residual matrix [2].

The magnetic behaviour of this type of nanomaterial was explained by the fact that the ferromagnetic exchange correlation length is greater than the α-Fe(Si) grain size [5,6]. The magnetocrystalline anisotropy is thus averaged out by the exchange interactions, as was previously pointed out in terms of the random anisotropy model [5–8]. It follows that the soft magnetic properties are determined by the average anisotropy which is several orders of magnitude lower than the magnetocrystalline anisotropy of the individual grains [6]. The low coercivity, high initial permeability and high saturation magnetization are due to a strong D^6 dependence of the anisotropy constant, where D is the mean diameter of the nanocrystallites [9]. Since the magnetic properties are related to both the microstructure and the phase composition, modifications in the magnetic properties are expected when a few percent of rare-earth is added.

*Corresponding author. Tel.: +33 2 35146766; fax: +33 2 35146652; e-mail: jean-marie.lebreton@univ-rouen.fr

0925-8388/97/$17.00
PII S0925-8388(97)00417-9

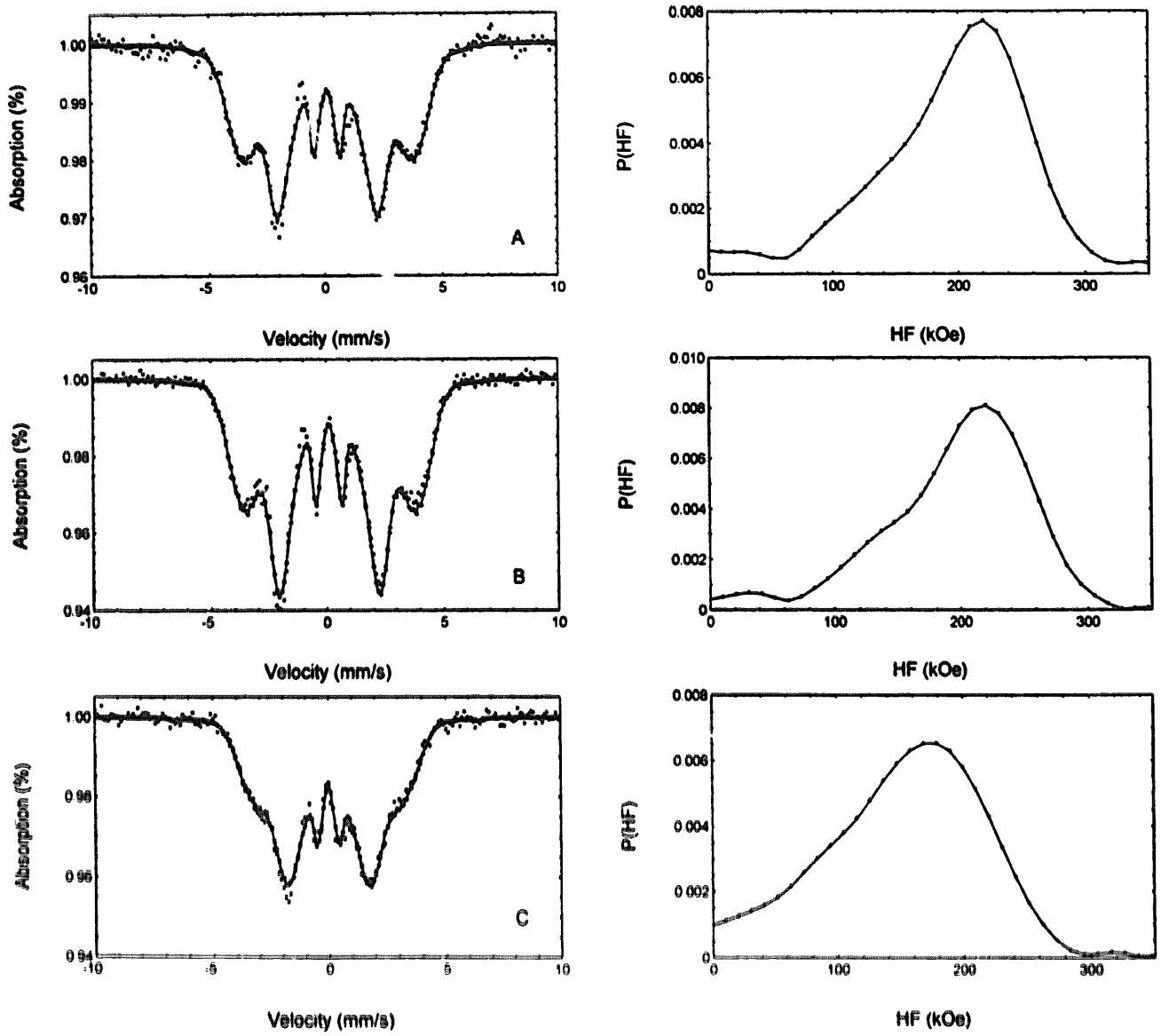

Fig. 1. Room temperature Mössbauer spectra and corresponding hyperfine field distributions of A, B and C samples.

In this paper we investigate the structural modifications induced by the addition of a few percent of Gd to amorphous and nanocrystallized ribbons of $Fe_{73.5}Cu_1Nb_3Si_{13.5}B_9$ nominal composition.

2. Experimental

Amorphous ribbons with nominal compositions $Fe_{73.5}Cu_1Nb_3Si_{13.5}B_9$ (A sample), $Fe_{73.5}Cu_1(Nb_2Gd)Si_{13.5}B_9$ (B sample) and $(Fe_{68.5}Gd_5)Cu_1Nb_3Si_{13.5}B_9$ (C sample) were obtained using a single roller melt spinning method, with a 40 cm diameter Cu roller and a 30 m/s speed corresponding to a 10^6 K/min cooling rate. The resulting as-quenched samples were annealed at several temperatures for several times, as follows:

As-quenched sample	Annealing temperature	Annealing time	Resulting sample
A	550°C	45 min	A1
A	600°C	24 h	A2
B	550°C	45 min	B1
C	550°C	45 min	C1
C	600°C	24 h	C2
C	600°C	30 min	C3
C	650°C	30 min	C4
C	720°C	30 min	C5

The thermal treatments were made under ultra-high vacuum to avoid oxidation. The structural properties of the samples were analyzed by means of transmission electron microscopy (TEM), X-ray diffraction (XRD) and Mössbauer spectrometry (MS). The TEM analysis was made on samples thinned by ion-etching

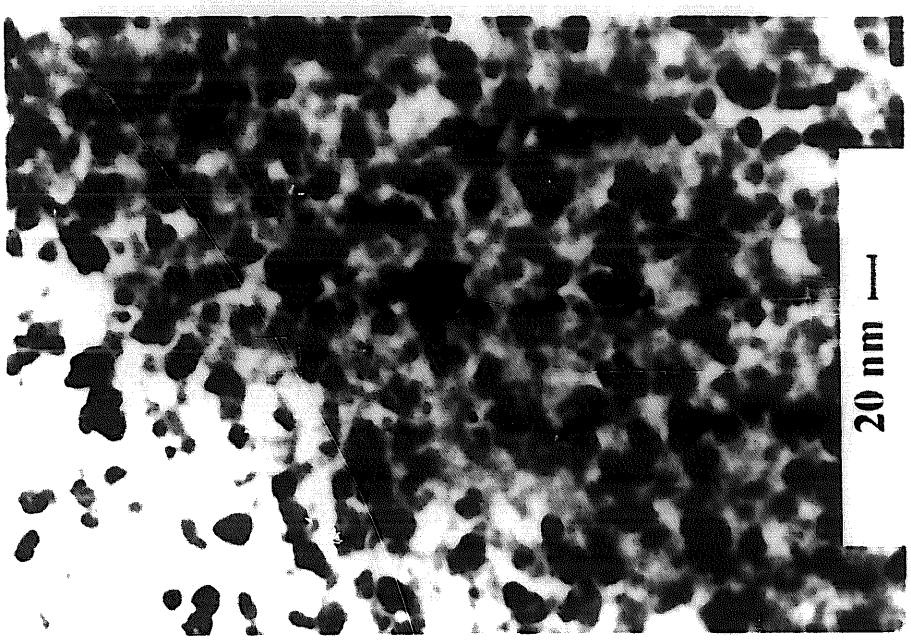

Fig. 2. TEM image of the A1 sample.

processes using a Philips C30 device. The XRD analysis was performed with a fast curved detector in an evacuated chamber. The X-ray generator was equipped with a Co anticathode, using Co Kα radiation ($\lambda = 0.17902$ nm). Transmission ^{57}Fe MS analyses were performed at room temperature with a conventional spectrometer using a ^{57}Co source in a rhodium matrix. The isomer shift (relative to metallic α-Fe at room temperature), quadrupolar splitting, quadrupolar shift and hyperfine field are denoted IS, QS, 2ε and HF, respectively. The relative Mössbauer intensity is denoted by A. Estimated errors Δ for the hyperfine parameters originate from the statistical errors σ given by the fitting procedure, taking $\Delta = 3\sigma$.

3. Results

3.1. The amorphous state

The XRD patterns of the as-quenched A, B and C samples reveal broad lines, typical for the amorphous state, with the maximum peak position at $\theta = 26°$ for both A and B samples and $\theta = 25.5°$ for C sample. The Mössbauer spectra of the as-quenched samples show very large lines, typical for the amorphous state, and were fitted with a distribution of magnetic sextets (Fig. 1). The mean hyperfine field values are 20.2 T, 19.5 T and 15.7 T, respectively, for the A, B and C

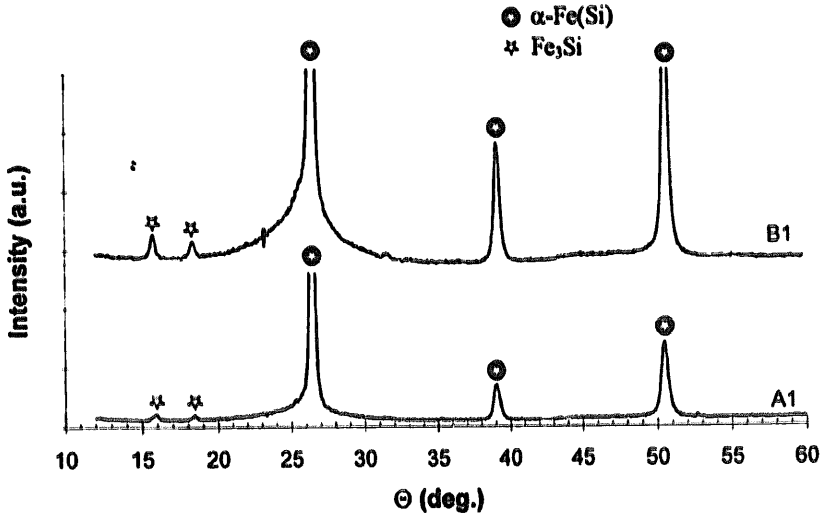

Fig. 3. XRD patterns of A1 and B1 samples.

Table 1
300 K Mössbauer hyperfine parameters for A1 and B1 samples

	A1 sample				B1 sample			
	IS (mm/s)	2ε (mm/s)	HF (T)	A (%)	IS (mm/s)	2ε (mm/s)	HF (T)	A (%)
Amorphous sextet	0.26	0.13	17.6	12	0.05	−0.01	17.3	12
α-Fe(Si): D + A_7 + A_8	0.07	−0.02	31.9	30	0.04	−0.01	31.5	29
α-Fe(Si): A_6	0.08	−0.01	28.9	18	0.07	0.00	28.7	13
α-Fe(Si): A_5	0.19	−0.01	24.7	22	0.16	0.00	24.7	23
α-Fe(Si): A_4	0.24	−0.02	20.1	17	0.22	−0.02	19.8	23

* The estimated errors are as follows: ±0.09 mm/s for 2ϵ, ±0.3 mm/s for QS, ±0.26 T for HF and ±1% for A.

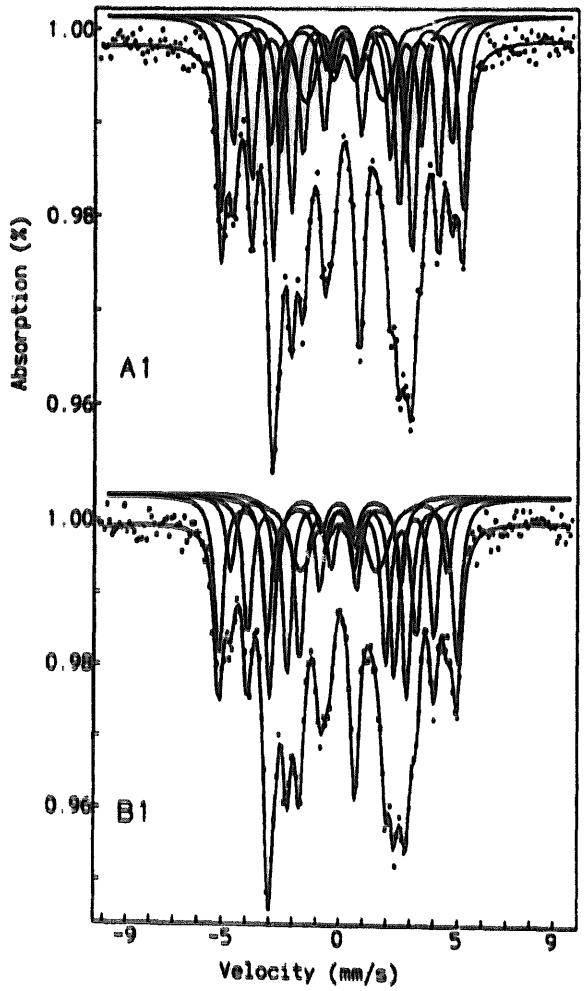

Fig. 4. Room temperature Mössbauer spectra of A1 and B1 samples. The contributions used to fit the spectra are displayed.

samples. It can be seen that Gd addition decreases the mean hyperfine field. This effect is related to both the spin polarization effects caused by the magnetic neighbours and the enhanced hybridization effects between the Fe 3d and Gd 5d orbitals [10].

3.2. The nanocrystalline state

3.2.1. Annealing at 550°C for 45 min

The A, B and C samples were heated at 550°C for 45 min. TEM observations reveal the presence of nanosized grains in both the A1 and B1 samples. The TEM image of the A1 sample is shown in Fig. 2. The mean grain sizes were estimated to 12 and 18 nm, respectively. The XRD patterns of A1 and B1 samples (Fig. 3) show sharp lines, corresponding to the (110), (200) and (211) reflections of the disordered body-centered-cubic (bcc) α-Fe(Si) structure. In both cases the unit cell parameter is (0.2842 ± 0.0002) nm. Some lines with weaker intensity that correspond to the ordered Fe_3Si solid solution are also observed, the unit cell parameter being (0.5680 ± 0.0002) nm. The α-Fe(Si) mean grain size was estimated by the Scherrer method [11] to be 12 nm and 21 nm, after instrumental broadening correction, for A1 and B1 samples, respectively. These values are in good agreement with those obtained from TEM observations.

The α-Fe(Si) nanocrystalline phase presents a DO_3-like structure. The ordered DO_3 structure consists of two types of sublattices: the D sublattice where each iron site has 8 Fe atoms as nearest neighbours and the A sublattice with A_n corresponding iron sites with $n = 4, 5, 6, 7$ and 8 iron atoms as nearest neighbours. The occupancy of the A_n iron sites depends on the Si content. As the Mössbauer contributions of the A_7 and A_8 sites have hyperfine magnetic fields close to that of the D site, only one component was used to fit the D, A_8 and A_7 sites contributions in the Mössbauer spectra. Thus, the room temperature Mössbauer spectra of A1 and B1 samples (Fig. 4) were fitted with four magnetic contributions corresponding to the α-Fe(Si) disordered phase and one broad magnetic sextet corresponding to the residual amorphous Fe-Nb-B phase. The fitted hyperfine parameters are reported in Table 1. The hyperfine fields of the α-Fe(Si) contributions are close to previously reported values [12,13]. These results are in agreement with both TEM and XRD data and indicate that A1 and B1 samples consist of nanosized grains of α-Fe(Si) embedded in an amorphous residual phase.

The XRD pattern for the C1 sample is similar to that of the as-quenched C sample, revealing the absence of the crystalline phase. This observation is

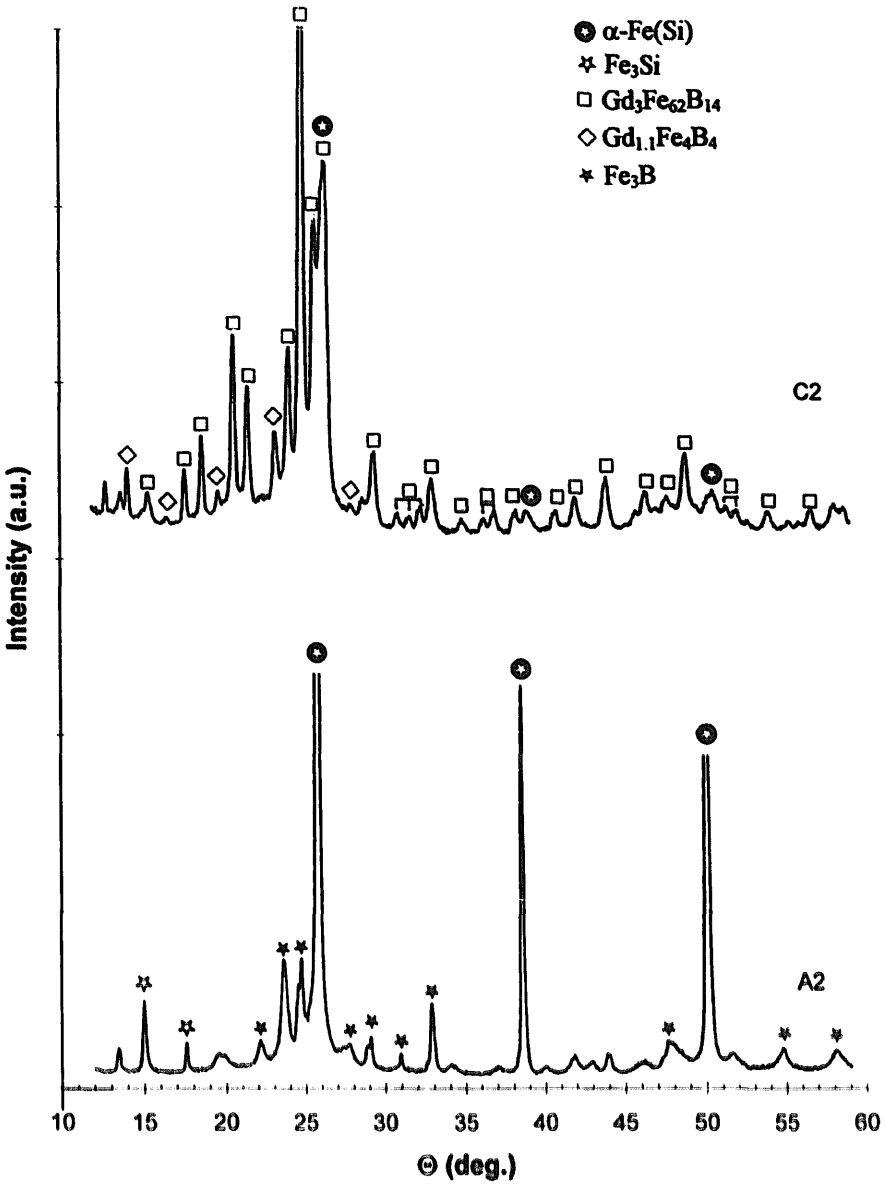

Fig. 5. XRD patterns of A2 and C2 samples.

Table 2
300 K Mössbauer hyperfine parameters for A2 and C2 samples

	A2 sample				C2 sample			
	IS (mm/s)	2ε, QS (mm/s)	HF (T)	A (%)	IS (mm/s)	2ε, QS (mm/s)	HF (T)	A (%)
α-Fe(Si): D + A_7 + A_8	0.05	0.01	32.0	27	0.11	−0.04	31.3	3
α-Fe(Si): A_6	0.09	0.02	29.2	7	0.13	0.08	29.3	3
α-Fe(Si): A_5	0.15	0.03	24.2	36	0.15	0.03	24.4	17
α-Fe(Si): A_4	0.25	−0.19	19.4	12	0.15	−0.06	19.1	7
Fe_3B: I	0.08	0.04	28.8	8	—	—	—	—
Fe_3B: II	0.00	0.05	26.6	2	—	—	—	—
Fe_3B: III	0.14	0.19	21.9	2	—	—	—	—
$Gd_3Fe_{62}B_{14}$: I	—	—	—	—	0.11	0.02	23.2	32
$Gd_3Fe_{62}B_{14}$: II	—	—	—	—	0.11	0.01	21.0	11
$Gd_3Fe_{62}B_{14}$: III	—	—	—	—	0.04	0.02	17.5	11
$Gd_3Fe_{62}B_{14}$: IV	—	—	—	—	0.05	0.02	15.5	11
Para Fe-Nb-B	0.16	0.27	—	7	0.16	0.27	—	1
Para $Gd_{1.1}Fe_4B_4$	—	—	—	—	0.06	0.56	—	5

*The estimated errors are as follows: ±0.03 mm/s for IS, ±0.05 mm/s for 2ϵ and QS, ±0.2 T for HF and ±1% for A.

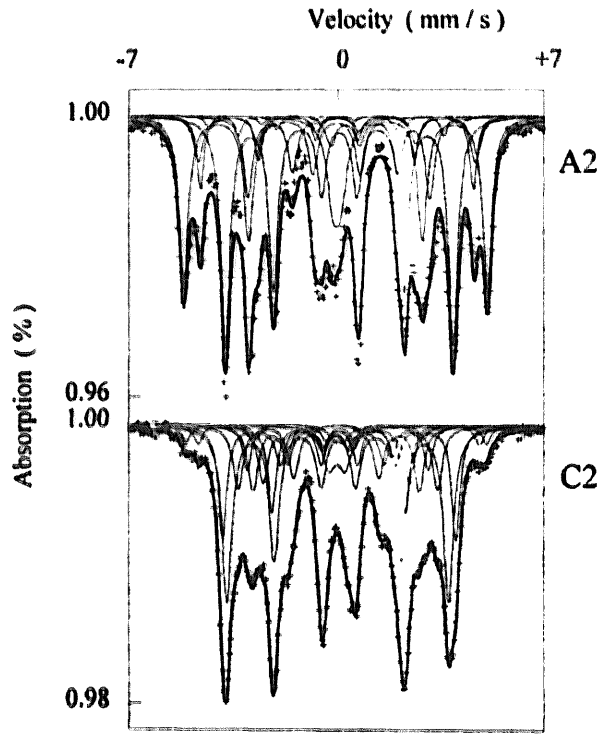

Fig. 6. Room temperature Mössbauer spectra of A2 and C2 samples. The contributions used to fit the spectra are displayed.

confirmed by the Mössbauer spectrum which consists of almost the same distribution of magnetic sextets (mean hyperfine field: 15.4 T) as that of the as-quenched C sample. This indicates that Gd addition increases the crystallization temperature of the amorphous phase. Annealings at higher temperatures are thus necessary to obtain further information about the development of phases induced by Gd addition.

3.2.2. Annealing at 600°C for 24 h

After annealing at 600°C for 24 h, the resulting A2 and C2 samples are completely crystallized. The XRD pattern of the A2 sample (Fig. 5) reveals the occurrence of the bcc α-Fe(Si) disordered phase with an increased mean grain size (as evidenced by sharper lines). Lines corresponding to the tetragonal Fe_3B phase are also observed. Other lines that have not been indexed could correspond to a residual Fe-Nb-B phase that crystallizes from the remaining amorphous matrix. The XRD pattern of the C2 sample (Fig. 5), shows the bcc α-Fe(Si) lines with a weaker intensity as compared to those of the A2 sample and the lines of the bcc $Gd_3Fe_{62}B_{14}$ metastable phase with a measured lattice parameter $a = (1.2192 \pm 0.0002)$ nm. The $RE_3Fe_{62}B_{14}$ metastable phase was also observed in alloys where RE = Nd [14], Y [15,16] and Dy [16]. Some lines corresponding to the tetragonal $Gd_{1.1}Fe_4B_4$ phase are also observed.

The Mössbauer spectrum of the A2 sample (Fig. 6) was fitted with four components corresponding to the α-Fe(Si) phase, as for the A1 sample, and three magnetic sextets corresponding to the tetragonal Fe_3B crystalline phase [10]. It is worth mentioning the occurrence of a paramagnetic component with a relative intensity of about 7% and a quadrupole splitting of (0.27 ± 0.05) mm/s, attributed to the Fe-Nb-B phase, that crystallizes from the amorphous matrix, in agreement with the XRD results. The fitted hyperfine parameters are reported in Table 2.

For the C2 sample, the four contributions of the bcc α-Fe(Si) phase were retrieved, with the same hyperfine fields than for the A2 sample (Table 2). The total relative intensity of the α-Fe(Si) contributions to the Mössbauer spectrum is lower for the C2 sample (30%) than for the A2 sample (82%). This indicates a reduction of the α-Fe(Si) amount in the C2 sample as compared with the A2 sample, in agreement with the XRD results. According to XRD results, the contribution of the $Gd_3Fe_{62}B_{14}$ is fitted. To our knowledge, no Mössbauer data of the $Gd_3Fe_{62}B_{14}$ metastable phase is available in the literature. However, as the $RE_3Fe_{62}B_{14}$ structure contains four different iron sites [17] the $Gd_3Fe_{62}B_{14}$ metastable phase contribution was fitted with four subspectra whose hyperfine fields are found to be in the 15–24 T range (Table 2). As no single phase $Gd_3Fe_{62}B_{14}$ material was obtained, a precise deconvolution of its Mössbauer contribution is difficult to perform. Thus, an assignment of the four Mössbauer contributions to the four iron sites was not made. The paramagnetic component attributed to the Fe-Nb-B phase is also observed, with a weaker intensity (1%) as compared to the A2 sample (7%). Another paramagnetic doublet with a relative proportion of about 5% and a quadrupole splitting of (0.56 ± 0.05) mm/s is found. This contribution is assigned to the $Gd_{1.1}Fe_4B_4$ phase, in agreement with XRD results.

3.2.3. Annealing at different temperatures for 30 min

In order to follow the evolution of the metastable phase in the C sample, annealings at different temperatures for 30 min were performed. The XRD pattern of the C3 sample shows that the alloy containing 5 at% Gd is mainly amorphous after annealing at 600°C for 30 min, as confirmed by MS. The presence of weak α-Fe(Si) lines indicates the beginning of the crystallization process (Fig. 7). The Mössbauer spectrum of the C3 sample (Fig. 8) was fitted taking into account a distribution of hyperfine fields. The mean hyperfine field value (16.5 T) is comparable to that of both C and C1 samples. The XRD patterns of the C4 and C5 samples annealed at 650°C and 720°C, respectively, exhibit the sharp lines of the bcc $Gd_3Fe_{62}B_{14}$

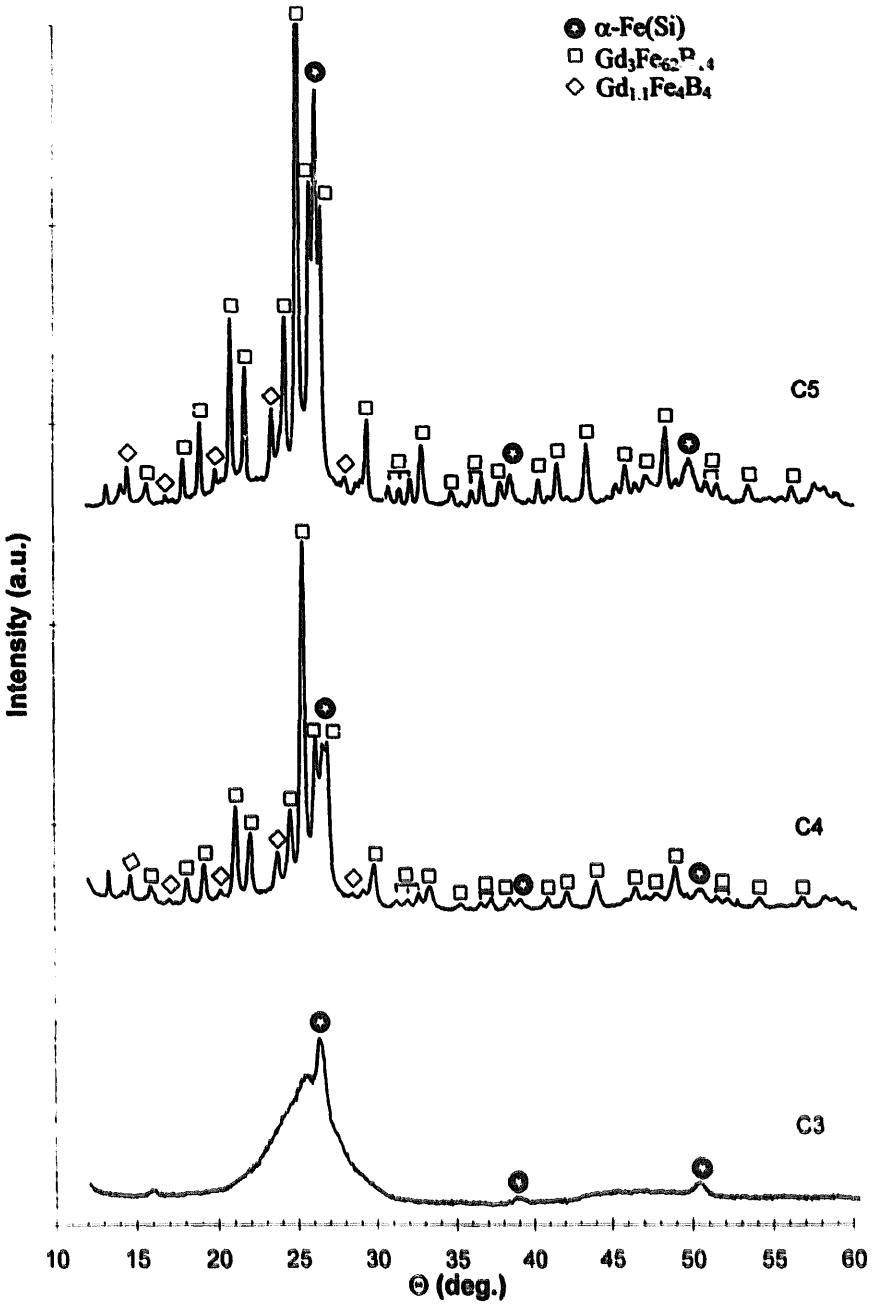

Fig. 7. XRD patterns of C3, C4 and C5 samples.

metastable phase with the same lattice parameter as for the C2 sample (Fig. 7). The $Gd_{1.1}Fe_4B_4$ and Fe-Nb-B phases are again identified.

From the fittings of the Mössbauer spectra of the C4 and C5 samples (Fig. 8) the hyperfine parameters related to the $Gd_3Fe_{62}B_{14}$ metastable phase are found to be close to those of the C2 sample (Table 3). The hyperfine fields of the four α-Fe(Si) sextets are also close to the values found for the other samples. As was observed for the C2 sample, a doublet corresponding to the paramagnetic $Gd_{1.1}Fe_4B_4$ phase is fitted in the Mössbauer spectra of both the C4 and C5 samples. For the C5 sample, a second doublet appears, its hyperfine parameters suggesting the paramagnetic Fe-Nb-B phase, as in the A2 and C2 samples, crystallized from the amorphous residual matrix.

4. Discussion

The truly initial amorphous state characterized by short-range magnetic order was checked for all the as-quenched samples by both XRD and MS results. The mean hyperfine field decreases when increasing the Gd content. Gd addition increases the crystallization temperature and in the alloy with 5 at% Gd content, the crystallization process begins at temperatures higher than 600°C.

It is shown that a 5 at% Gd addition modifies the

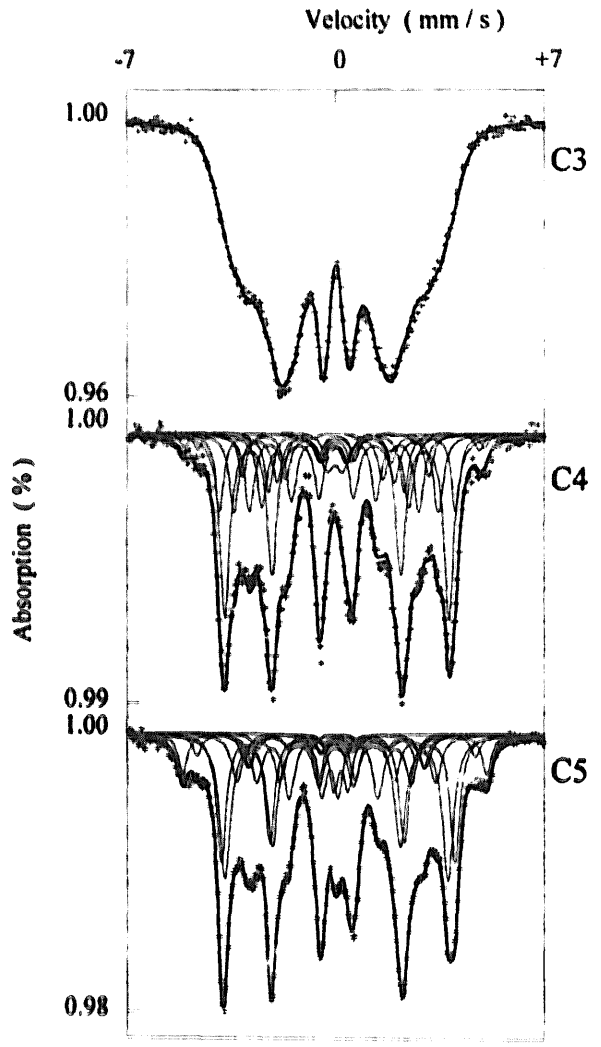

Fig. 8. Room temperature Mössbauer spectra of C3, C4 and C5 samples. The contributions used to fit the spectra are displayed.

microstructure of Fe-Cu-Nb-Si-B alloys by forming Gd-Fe-B phases. The bcc $Gd_3Fe_{62}B_{14}$ metastable phase with a unit cell parameter $a = (1.2192 \pm 0.0002)$ nm and the paramagnetic $Gd_{1.1}Fe_4B_4$ phase were observed. The results indicate that the combined effects of annealing time and temperature determine the crystallization and growth of the α-Fe(Si) and $Gd_3Fe_{62}B_{14}$ phases. On annealing at 600°C, the α-Fe(Si) phase is first formed and then the $Gd_3Fe_{62}B_{14}$ metastable phase crystallizes. On annealing at higher temperatures, the relative amounts of the two phases vary, such that an increase of the α-Fe(Si) amount is observed together with a decrease of the $Gd_3Fe_{62}B_{14}$ amount. This behaviour suggests that the $Gd_3Fe_{62}B_{14}$ metastable phase transforms into α-Fe and $Gd_{1.1}Fe_4B_4$ as a slight increase of the $Gd_{1.1}Fe_4B_4$ amount is observed. Further studies are required to investigate the possible formation of stable magnetic Gd-Fe-B phases from the $Gd_3Fe_{62}B_{14}$ metastable phase transformation. The Mössbauer contribution of the $Gd_3Fe_{62}B_{14}$ metastable phase was fitted using four sextets with consistent hyperfine parameters throughout the series of spectra.

On annealing the A and C samples at 600°C for long times or at higher temperatures (720°C) for a short time, a paramagnetic component is observed in the Mössbauer spectra. This component is associated with an Fe-Nb-B phase, in agreement with published results [12,13]. This phase would crystallize from the residual amorphous phase.

As Gd addition induces structural modifications by the formation of Gd-Fe-B phases, modifications of the magnetic properties are expected. The investigation of the magnetic properties of these samples is developed elsewhere [18].

5. Conclusions

The nanocrystalline phases resulting from the appropriate annealing of the $Fe_{73.5}Cu_1Nb_3Si_{13.5}B_9$ ribbons doped with few percent of Gd, were studied using TEM, XRD and Mössbauer analyses. The presence of 5 at% Gd in the as-quenched sample, lowers

Table 3
300 K Mössbauer hyperfine parameters for C4 and C5 samples

	C4 sample				C5 sample			
	IS (mm/s)	2ε, QS (mm/s)	HF (T)	A (%)	IS (mm/s)	2ε, QS (mm/s)	HF (T)	A (%)
α-Fe(Si): D + A_7 + A_8	0.11	−0.11	31.1	3	0.08	−0.06	31.5	7
α-Fe(Si): A_6	0.13	0.12	29.2	2	0.13	−0.05	28.9	4
α-Fe(Si): A_5	0.13	0.03	24.5	12	0.15	0.03	24.3	22
α-Fe(Si): A_4	0.12	−0.08	19.4	6	0.13	−0.24	18.0	4
$Gd_3Fe_{62}B_{14}$: I	0.12	0.01	23.3	33	0.11	0.00	23.2	28
$Gd_3Fe_{62}B_{14}$: II	0.10	0.02	21.3	13	0.11	−0.03	20.7	10
$Gd_3Fe_{62}B_{14}$: III	0.04	0.00	17.7	13	0.16	−0.10	18.5	5
$Gd_3Fe_{62}B_{14}$: IV	0.06	0.04	15.4	14	0.02	0.00	16.2	11
Para Fe-Nb-B	—	—	—	—	0.16	0.27	—	3
Para $Gd_{1.1}Fe_4B_4$	0.06	0.56	—	4	0.06	0.56	—	6

* The estimated errors are as follows: ±0.02 mm/s for IS, ±0.03 mm/s for 2ε and QS, ±0.2 T for HF and ±1% for A.

the mean hyperfine field and increases the crystallization temperature. For all the crystallized samples the Mössbauer hyperfine parameters of the α-Fe(Si) contribution are similar. The variations in the α-Fe(Si) amount, obtained from Mössbauer spectrometry, are caused by Gd addition, increasing annealing temperature and annealing time. The $Gd_3Fe_{62}B_{14}$ metastable phase was observed in all the crystallized samples containing 5 at% Gd. Four magnetic Mössbauer components corresponding to the four different iron sites were fitted and their hyperfine field values were obtained. The $Gd_{1.1}Fe_4B_4$ and a residual Fe-Nb-B paramagnetic phases were also observed and characterized in both XRD and MS spectra.

Acknowledgements

The authors wish to thank the Romanian Ministry of Research and Technology for the financial support under contracts no. 33/A7 and 33/A22. The financial support of the Ministère Français des Affaires Etrangères, Centre National de la Recherche Scientifique and Centre International des Etudiants et Stagiaires, in the frame of the 'Formation Recherche' program 90RO933 no. 152309L, is also gratefully acknowledged.

References

[1] Y. Yoshizawa, S. Oguma, K. Yamauchi, J. Appl. Phys. 64 (1988) 6044.
[2] G. Herzer, IEEE Trans. Magn. 25 (1989) 3327.
[3] H.K. Lachowicz, A. Slawska-Waniewska, J. Magn. Magn. Mater. 133 (1994) 238.
[4] A. Slawska-Waniewska, M. Gutowski, H.K. Lachowicz, T. Kulik, H. Matyja, Phys. Rev. B46 (1992) 14594.
[5] A. Hernando, T. Kulik, Phys. Rev. B49 (1994) 7064.
[6] G. Herzer, Mater. Sci. Eng. A133 (1991) 1.
[7] R. Alben, J.J. Becker, M.C. Chi, J. Appl. Phys. 49 (1978) 1653.
[8] G. Herzer, J. Magn. Magn. Mater. 112 (1992) 252.
[9] G. Herzer, IEEE Trans. Magn. 26 (1990) 1397.
[10] A. Jianu, O. Crisan, V. Kuncser, J.M. Le Breton, J. Teillet, E. Vasile, C. Munteanu, G. Filoti, Mater. Sci. Eng. (1997) (in press).
[11] H.P. Klug, L.A. Alexander, X-ray Diffraction Procedures for Polycrystalline and Amorphous Materials, John Wiley, New York, 1974.
[12] G. Hampel, A. Pundt, J. Hesse, J. Phys. Condens. Matter 4 (1992) 3195.
[13] M. Garcia del Muro, R. Zquiak, X. Batlle, J. Parellada, J. Magn. Magn. Mater. 140–144 (1995) 475.
[14] Z. Altounian, D.H. Ryan, G.H. Tu, J. Appl. Phys. 64 (1988) 5723.
[15] K.H.J. Buschow, D.B. de Mooij, R. Coehoorn, J. Less-Common Metals 80 (1989) 101.
[16] Z. Cheng, M. Mao, J. Sun, et al., J. Phys. Condens. Matter 7 (1995) 2303.
[17] D.C. de Mooij, J.L.C. Daams, K.H.J. Buschow, Philips J. Res. 42 (1987) 339.
[18] O. Crisan, J.M. Le Breton, M. Noguès, A. Jianu, J. Teillet, G. Filoti, to be presented at 'Soft Magnetic Materials 13', Grenoble, France, 24–26 Sept. 1997.